NUMERICAL SIMULATION OF MESOSCALE STRUCTURES OF TYPHOON AND OROGRAPHIC EFFECTS USING MM5*

Wang Pengyun (王鹏云)

Chinese Academy of Meteorological Sciences, Beijing 100081

Received April 22, 1999; revised July 10, 1999

ABSTRACT

The track, landfall, dynamic and thermodynamic and cloud-rain physical mesoscale structures and their evolution of typhoon HERB 1996 in 36 h from 0000 UTC 31 July to 1200 UTC 1 August 1996 were simulated by using the non-hydrostatic mesoscale model MM5. This period covered the process of typhoon HERB landfall at Taiwan and Fujian Provinces.

Results show that the model successfully simulated the landfall process of typhoon HERB, revealed the most important characteristics of the mesoscale dynamic and thermodynamic and cloud-rain physical structure during its landfall. The simulated typhoon track was close to the observation. The center of cyclonic circulation simulated at 0000 UTC on 1 August 1996 (24 h integration) was located in shore near Fuqing, Fujian Province at which the typhoon was reported to landfall two hours later. It shows that strong upward motion formed by low level convergence existed in the eye-wall and subsidence at the eye. The wind field shows clear asymmetrical structure near the typhoon center. The cloud and rainband was screw-typed distributed around typhoon center, and consisted of meso-β scale rain cores. During the period of typhoon HERB staying near and passing over Taiwan, the lower cloud was developed in the eye region so that the previous clear typhoon eye on the satellite pictures became fuzzy. Observation shows that the typhoon center was "warm", but the model simulations with higher space resolution show that in the mid-troposphere the region of eye-wall with stronger upward motion and more cloud- and rain-water was warmer than the eye.

During the period of typhoon passing over Taiwan and its following landfall at Fujian, the track of model typhoon deviated about 30 km northward (i. e., rightward) because of the orographic effects of Taiwan Island, but the strength of the typhoon was not affected remarkably. The amount of rainfall on Taiwan in the 36 h simulations was enhanced more than six times by the orographic lifting of Taiwan Mountain.

Key words: typhoon, mesoscale, cloud physical structure, orographic effects, MM5 (mesoscale model, version 5)

I. INTRODUCTION

The tropical storm No. 9608 was formed on 24 July 1996, and then developed into typhoon (HERB 1996) on 26 July in the Northwest Pacific Ocean and moved westward. After passing over the north region of Taiwan on 31 July, it landed at Fuqing, Fujian

* Supported by the Program of "Research on the Formation Mechanism and Prediction Theory of Severe Synoptic Disasters in China" (G1998040907).

Province of South China at 0230 UTC 1 August 1996. After landfall. it moved northwestward and weakened into tropical storm in Jiangxi Province in the afternoon of 1 August. The wind speed maximum up to 40—60 m s^{-1}, and heavy rainfall of 1987 mm at Alishan, 653 mm at Riyuetan, Taiwan were reported during the typhoon landfall and staying at Taiwan from 30 July to 1 August. The strong wind and heavy rainfall made 20 people died, 40 missed and hundreds injured. It was estimated that over one billion U.S. dollars of property was damaged in Taiwan.

The cyclone decayed from the landfall typhoon continually moved northwestward, passing over Jiangxi, Hunan, Hubei, Henan, Shanxi and Shaanxi Provinces. Under the influence of the cyclone, heavy rain fell in many places on its way. More than 100 mm rainfall fell in north Hubei and 200 mm in Hanshui River reaches. In Shaanxi Province, 1.3×10^4 ha of agricultural field was flooded, one bridge was broken, highway 310 was broken off, and tens of thousand people were besieged by flood.

During the typhoon HERB passing over Taiwan, the previous clear typhoon eye shown on the satellite infrared cloud pictures was becoming fuzzy, that made the forecasters difficult to locate the typhoon center (Fig. 1). Liu et al. (1998) have analyzed some of the dynamic and thermodynamic structures associated with this typhoon by using the typhoon numerical model of National Meteorological Center (NMC), but this model is a hydrostatic operational one so their study was limited on a larger scale.

Moreover, since Taiwan Mountain (also known as Zhongyang Mountain) with most

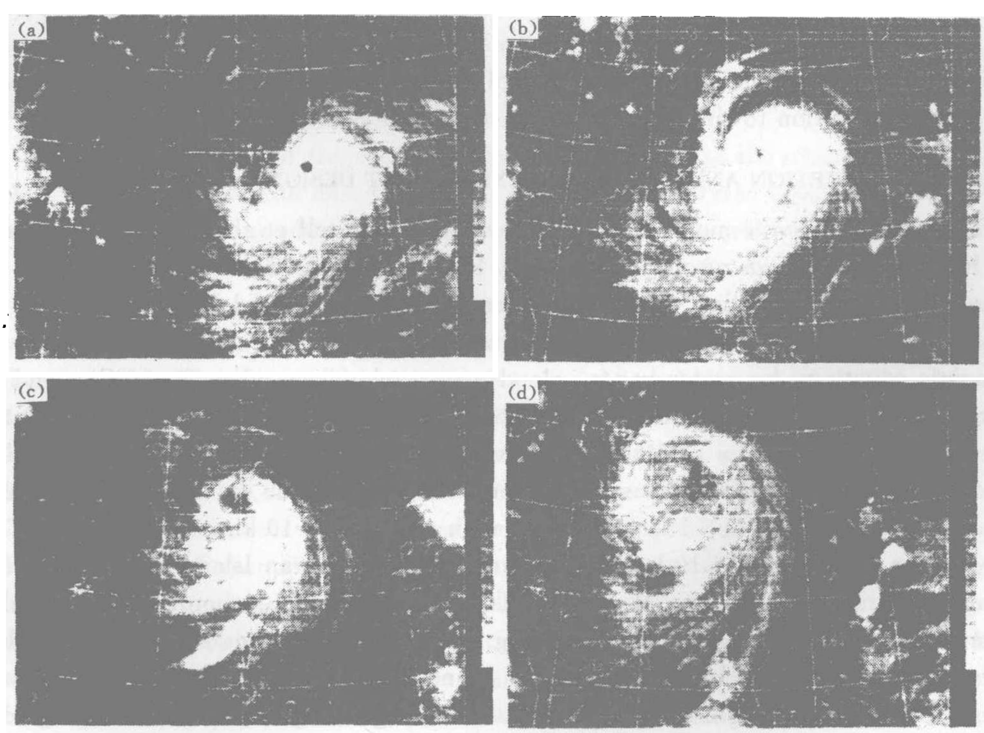

Fig. 1. Satellite infrared cloud picture. (a) 2330 UTC 30 July; (b) 1230 UTC 31 July; (c) 0030 UTC 1 August; (d) 1230 UTC 1 August.

of its peaks above 3000 m is oriented from north to south on central Taiwan Island, it may affect the structures and rainfall of typhoon when the typhoon closing to or landing at and passing over the island. Previous studies have shown that the orography of Taiwan Island had remarkable effects on the track, strength and structures of typhoons when they passed over Taiwan Island or nearby ocean and then landed on Fujian or Zhejiang Provinces (e.g., Brand and Blelloch 1974; Chang 1982; Bender et al. 1987; Yeh and Elsberry 1991; Luo and Chen 1995). In recent years, some mesoscale model simulations have done to study the orography effects of the island on typhoons, for example, secondary cyclonic circulation center formed in the west rear of the island and the deviation of typhoon track when typhoons moved to the east of Taiwan Island (Men et al. 1996; Yong et al. 1996). Some studies on the orographic effects of the island on typhoon induced heavy rainfall were also done, but most of them used idealized symmetric terrain data instead of real terrain data (Hamuro et al. 1969; Bender et al. 1985). Zheng and Wu (1996) simulated the orography effects on "9216" typhoon induced rain enhancement using real terrain data, but their study was mainly concentrated on the effects over the mainland when the typhoon landed on the Fujian Province.

For gaining insight into both dynamic and thermodynamic structures and cloud and rain physical structures near typhoon center in mesoscale, and the orographic effects of Taiwan Island on heavy rainfall at Taiwan, in this paper, we will present numerical studies by using a non-hydrostatic mesoscale model MM5 with high resolution (10—30 km of grade spacing). The study will be focused on the period of landfall at Taiwan and Fujian from 0000 UTC 31 July to 1200 UTC 1 August 1996.

This study is also a test for the ability of the non-hydrostatic mesoscale model MM5 with higher resolution to simulate and forecast landfall typhoons.

II. MODEL DESCRIPTION AND NUMERICAL EXPERIMENT DESIGN

The non-hydrostatic model MM5 was described by Grell et al. (1994). The version used here includes a high-resolution planetary boundary layer. Experiments including four choices to treat precipitation physics and terrain effects are listed in Table 1. AK used Anthes-Kuo cumulus parameterization scheme; EXPL30 used explicit scheme in which prognostic equations for water vapor, cloud water (cloud ice when $T<0°C$), and rain water (snow when $T<°C$) were included. The domain (centered at 26°N, 118°E) contains 61×61 grid points with a grid size of 30 km for both AK and EXPL30. In EXPL10, explicit scheme and Grell cumulus parameterization were used. Its domain (centered at 26°N, 119°E) contains 121×121 grid points with grid size of 10 km. In EXPL10-NT, all choices were same as EXPL10 but the terrain effects of Taiwan Island were excluded for testing the orographic effects of Taiwan Island on typhoon structure and rainfall at Taiwan, which was carried out by reducing the terrain height data on model grids on Taiwan to 0.1 m with the land feature on the island kept. In all experiments, the terrain is represented by actual height on a $10'\times10'$ latitude-longitude grid and analyzed on grids by using 16 points and two dimension parabolic interpolations; the model atmosphere is divided into 25 layers from surface to 10 hPa; a sigma coordinate system is used. The model was initiated using the grid data (grid spacing 1.875° of latitude/longitude) of NMC medium range spectral model T63 as a "first guess" field, supplemented by operational surface and rawinsonde data, and sea surface temperature and land use data. The time-dependent inflow-outflow conditions were used for lateral boundary, and the data at boundary were linearly interpolated at 12 h intervals in time by using T63 analyses and observational data. The model simulations were started at 0000 UTC 31 July and ended at 1200 UTC 1 August 1996 for total 36 h.

Table 1. List of Simulation Experiments

Experiment name	Description	Grid size and points of domain
AK	Anthes-Kuo cumulus parameterization scheme	30 km, 61×61
EXPL30	Explicit scheme	30 km, 61×61
EXPL10	Explicit scheme and Grell cumulus parameterization scheme	10 km, 121×121
EXPL10-NT	Same as EXPL10 but no orographic effects of Taiwan Island	10 km, 121×121

III. COMPARISON OF MODEL NUMERICAL SIMULATIONS AND OBSERVATIONS

The comparison of simulations and observations shows that MM5 simulated the track of typhoon HERB and its induced rainfall quite well during its landfall at Taiwan and Fujian, no matter what experiments shown in Table 1 were used.

1. *Track of Typhoon and Landfall at Fujian Province*

The simulated track of the typhoon was generally close to the observations. Lacking of observational data on the East China Sea, the initially analyzed typhoon center was 130 km to southeast from the observation, and its strength was weaker than the observation: sea-level pressure at the center of initial typhoon was 985 hPa, 45 hPa higher than observed 940 hPa. As a result, the simulated typhoon track was deflected to the south and the typhoon center was delayed in the first 12 hours. However, the simulated typhoon track was adjusted by the model itself and closed to the observations gradually. After 24 h model integration, at 0000 UTC 1 August, shown in Table 2, the simulated locations of typhoon center are quite close to the observations for all the experiments, for example, 25. 2°N, 119. 7°E for EXPL30 and 25. 6°N, 120. 3°E for EXPL10 become comparable with 25. 4°N, 120. 0°E for observations. Two hours and thirty minutes later the typhoon was landed at Fuqing, Fujian Province for both observations and simulations. Although the strength of the simulated typhoon was still weaker than that of the observation, the difference of sea-level pressure at typhoon center had been reduced from initial 45 hPa to 21—24 hPa for all the experiments. The general evolution trend of the strength, decaying during the 36 h period, was also simulated well by the model.

Table 2. Comparison of Simulated 36 h Rainfall and Location of Typhoon Center at 0000 UTC 1 August 1996 (24 h Integration) with Various Experiments, Objective Analyses (OBJANS) and Observational Reports (OBS)

Simulation experiments	Total rainfall in 36 h from 0000 31 July to 1200 1 August (mm)		Location of typhoon center (Latitude/Longitude)	Sea-level pressure at typhoon center (hPa)
	At Taiwan	At Fujian		
AK	463	94	25.4°N/120.6°E	992
EXPL30	224	57	25.2°N/119.7°E	994
EXPL10	269		25.6°N/120.3°E	992
EXPL10-NT	40		25.4°N/120.4°E	991
OBJANS			24.7°N/120.3°E	982
OBS	Alishan:	Fuzhou:	25.4°N/120.0°E	970
	1987*:	158:		
	Riyuetan:	Xiamen:		
	653*	63		

* Total rainfall during periods from 30 July to 1 August 1996.

2. *Rainfall*

The 36 h accumulated rainfall simulated by all four experiments is shown in Fig. 2. The pattern of rainfall distribution shown in Figs. 2a, 2b and 2c is similar to that shown on the satellite infrared cloud picture (Fig. 1), and the maximum rainfall on north Taiwan shown in Fig. 3 is also revealed from the simulations: 463 mm from AK, 224 mm from EXPL30, and 269 mm from EXPL10. However, the maximum rainfall on Taiwan simulated by EXPL10-NT was only 40 mm, about one sixth of EXPL10. This will be discussed in Section VI.

Among these experiments, AK simulated rainfall amount and distribution are more close to observations. The rainfall predicted by Anthes-Kuo cumulus parameterization scheme includes two parts: one is large-scale non-convective rain and the other is convective rain. Results in this case show that the two parts had equal contribution to the total rainfall. On the north part of Taiwan near the typhoon center, the total 463 mm rainfall consisted of 274 mm convective rain and 189 mm non-convective rain, but the maximum rainfall at south Taiwan was mainly from covective rain. The EXPL30 predicted similar pattern of rainfall distribution, but the maximum at north Taiwan was only half of that by AK. This may be caused by the fact that EXPL30 considered only resolvable scale (scale$\geqslant$30 km) precipitation, but did not consider the non-resolvable scale or sub-scale (scale$<$30 km) convective rain. In EXPL10, both resolvable scale (scale$\geqslant$10 km) rain

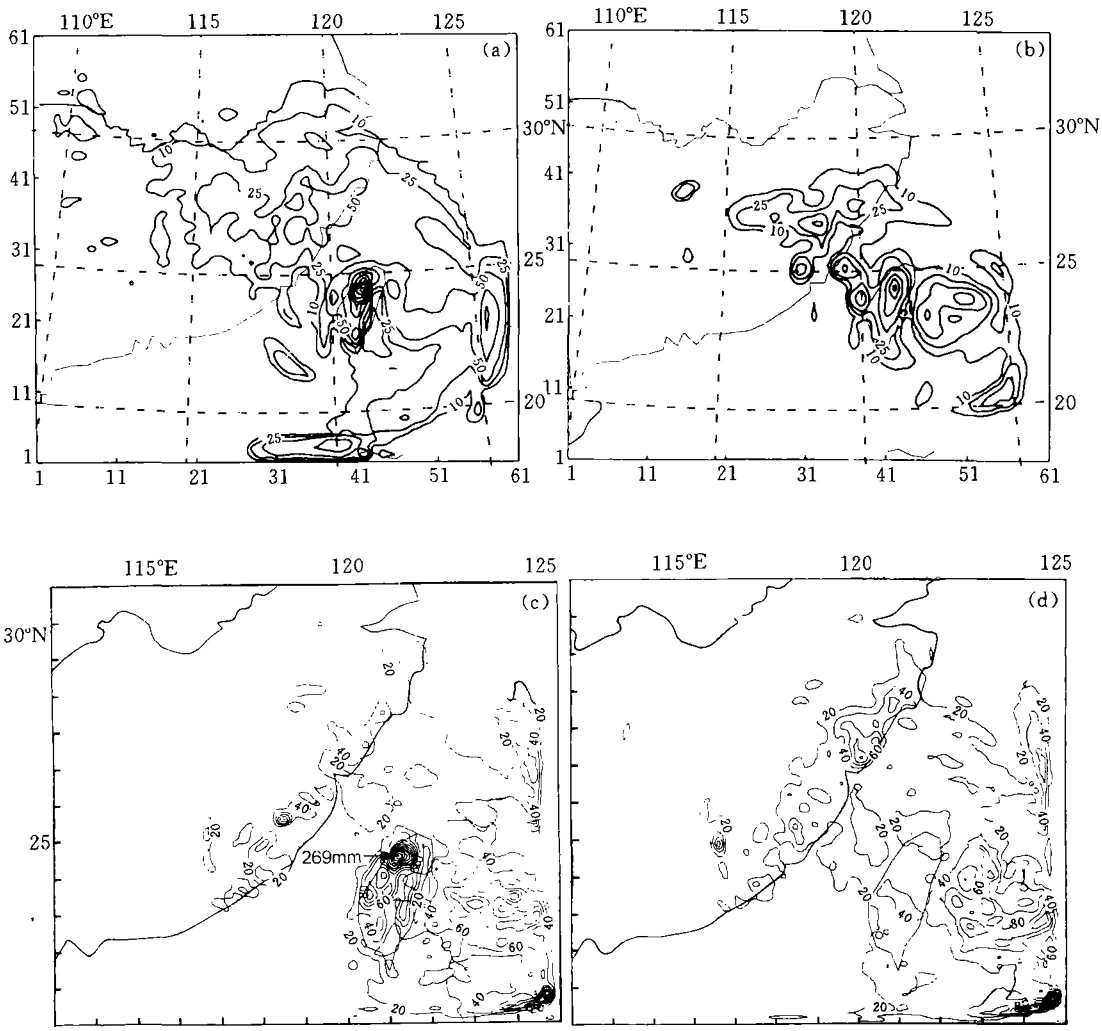

Fig. 2. Model simulated 36 h rainfall. (a) AK; (b) EXPL30; (c) EXPL10; (d) EXPL10-NT. Continuous contours denote 10, 25, 50, 100, 150, 200, 250, 300, 350, 400, 450, 500 mm for (a) and (b); contours with intervals of 20 mm are drawn for (c) and (d).

and non-resolvable scale or sub-scale (scale<10 km) convective rain were involved, but results show that the rainfall predicted by EXPL10 was mainly composed of resolvable scale rain. The above discussion indicates that the convection scale near the typhoon center was 10—30 km. Therefore, simulation with grid spacing equal to or larger than 30 km must consider sub-scale cumulus parameterization.

Since the experiments of EXPL30 and EXPL10 include explicit treatment of cloud water, rain water, snow and ice, they can provide not only the dynamic and thermodynamic structures but also the cloud and precipitation distributions near typhoon center. Therefore, we will use these two experiments in the following sections for analyzing the structures, development and evolution of typhoon HERB, and EXPL10 and

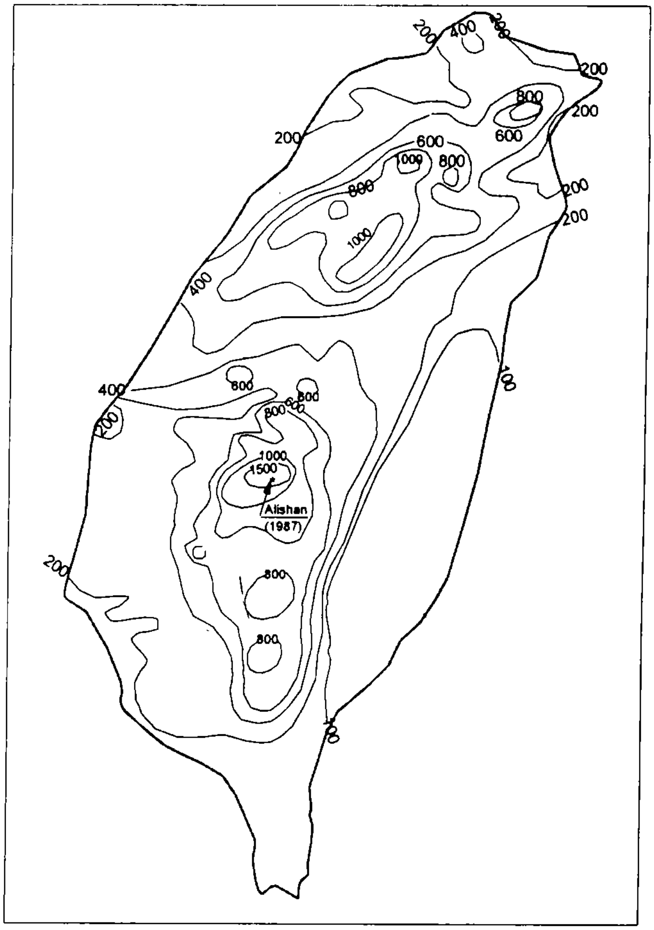

Fig. 3. Total rainfall observed at Taiwan from 30 July to 1 August 1996. Contours labeled in mm.

EXPL10-NT for testing the orographic effects of Taiwan Island on the heavy rainfall induced by the typhoon.

IV. DYNAMIC AND THERMODYNAMIC STRUCTURES AND EVOLUTION OF TYPHOON HERB DURING ITS LANDFALL AT TAIWAN AND FUJIAN

1. *Structure of Circulation near Typhoon Center*

From a series of typhoon track analyses Chen (1985) concluded that asymmetrical structure of typhoon could greatly impact its motion direction. Analyses and numerical simulations using data from intensified observations of experiments SPECTRUM, TCM-90 and TYPHOON in summer 1990 at Northwest Pacific Ocean verified this point of view (Chen and Luo 1996; Luo et al. 1996; Xu et al. 1996).

Our simulations clearly show cyclonic circulation and asymmetrical structure near the typhoon center. Examining the circulation fields at 25 pressure levels from 1000 hPa up to 10 hPa we can see that the cyclonic circulation extends from surface up to 200 hPa, and cyclonic inflow is below and outflow above 450—600 hPa near the center. Figure 4 shows streamline fields at 0000 UTC 1 August 1996 (24 h integration) at 850, 700 and 500 hPa,

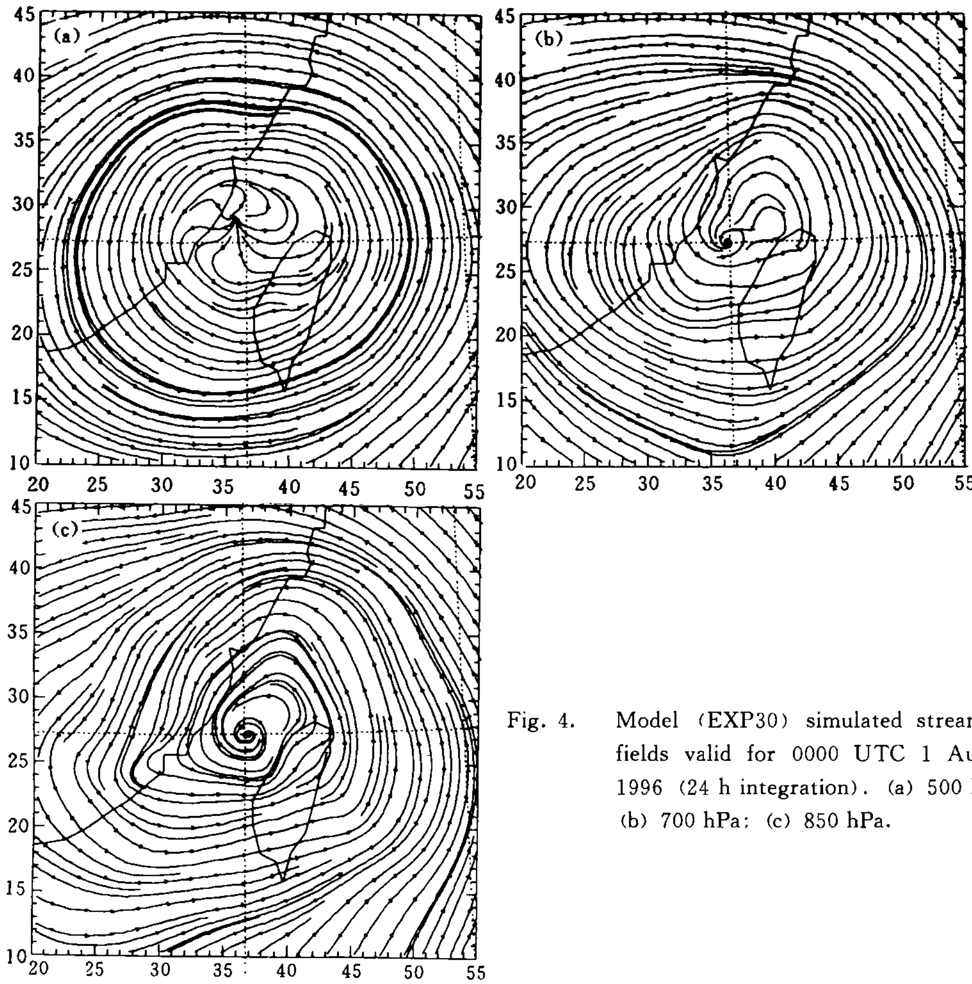

Fig. 4. Model (EXP30) simulated streamline fields valid for 0000 UTC 1 August 1996 (24 h integration). (a) 500 hPa; (b) 700 hPa; (c) 850 hPa.

respectively, simulated by EXPL30. It clearly shows cyclonic circulation at the three pressure levels, outflow from typhoon center at 500 hPa, and inflow towards typhoon center at 850 and 700 hPa. Simulations by EXPL10 with higher resolution than by EXPL30 show similar results, except that the changing level from inflow to outflow happens near 450 hPa. Figures 5a and 5c show the geopotential height field superimposed by wind field at 850 hPa and 700 hPa, respectively. The wind was stronger in the northeast quadrant of the center and weaker in the southwest, such a pattern of wind field and the westward moving of the typhoon are consistent with the conclusion of Chen and Luo (1996).

Vertical cross section of vorticity along AB on Fig. 5d shows vorticity maximum, $2.8 \times 10^{-4}\ s^{-1}$, located at 800 hPa in the north part of typhoon eye-wall; and at 950 hPa in the south part. In the eye of typhoon, vorticity was weak (figure omitted).

Vertical velocity ω is directly integrated from vertical momentum equation:

$$\frac{\partial P^* \omega}{\partial t} = - m^2 \left[\frac{\partial P^* u\omega/m}{\partial x} + \frac{\partial P^* v\omega/m}{\partial y} \right] - \frac{\partial P^* \dot{\sigma} \omega}{\partial \sigma} + \omega DIV$$

$$+ P^* g \frac{\rho_0}{\rho}\left[\frac{1}{P^*}\frac{\partial P'}{\partial \sigma} + \frac{T'_v}{T} - \frac{T_0 P'}{T P_0}\right] - P^* g[q_c + q_r] + D_\omega,$$

where pressure P, temperature T and density ρ consist of constant reference state P_0, T_0, ρ_0 and corresponding perturbations P', T', ρ', i.e.,

$$P(x, y, z, t) = P_0(z) + P'(x, y, z, t),$$
$$T(x, y, z, t) = T_0(z) + T'(x, y, z, t),$$
$$\rho(x, y, z, t) = \rho_0(z) + \rho'(x, y, z, t).$$

The vertical σ-coordinate is defined entirely from the reference pressure $\sigma = (P_0 - P_t)/P^*$, where $P^*(x, y) = P_s(x, y) - P_t$. P_s and P_t are the surface and top pressures, respectively, of the reference state and independent of time.

Term D_ω represents the vertical and horizontal diffusion and vertical mixing due to the planetary boundary layer turbulence. DIV term is divergence added for the non-hydrostatic equation.

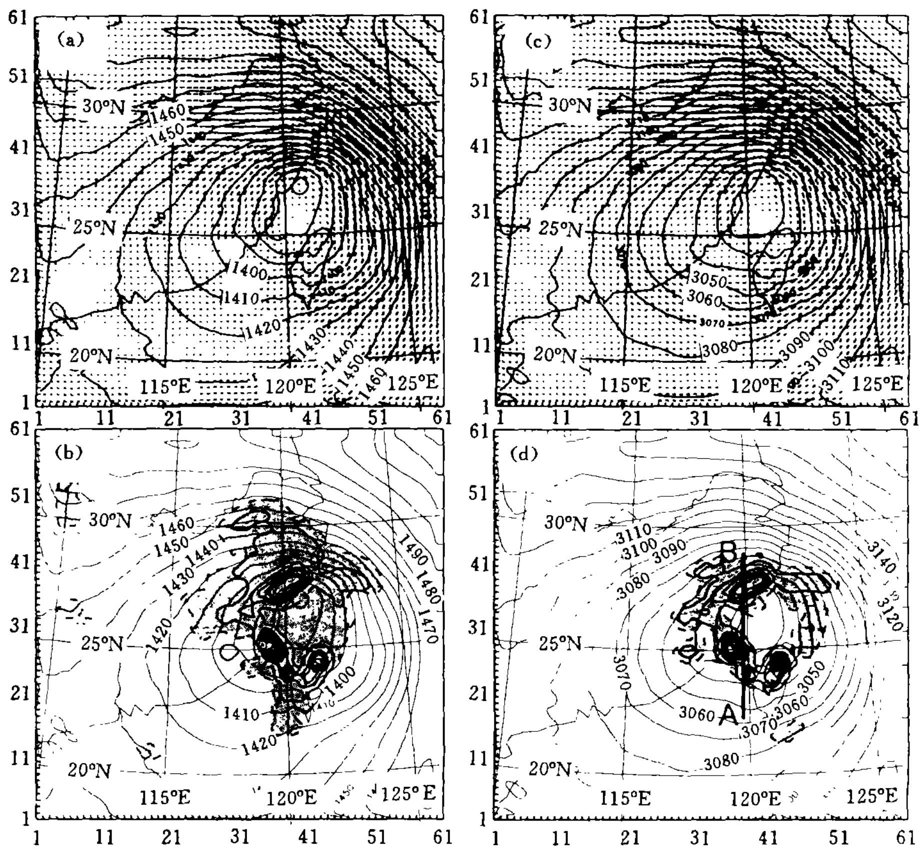

Fig. 5. Model (EXP30) simulated at 0000 UTC 1 August 1996: (a) geopotential height (gpm) and wind field at 850 hPa; (b) geopotential height, cloud water mixing ratio (shaded area represents $\geqslant 1.0\times10^{-5}$ kg kg^{-1}) and rain water mixing ratio (heavy contoured lines with an initial value of 1.0×10^{-5} kg kg^{-1} and then at increasing intervals of 10×10^{-5} kg kg^{-1}); (c) same as (a) but for 700 hPa; (d) same as (b) but for 700 hPa.

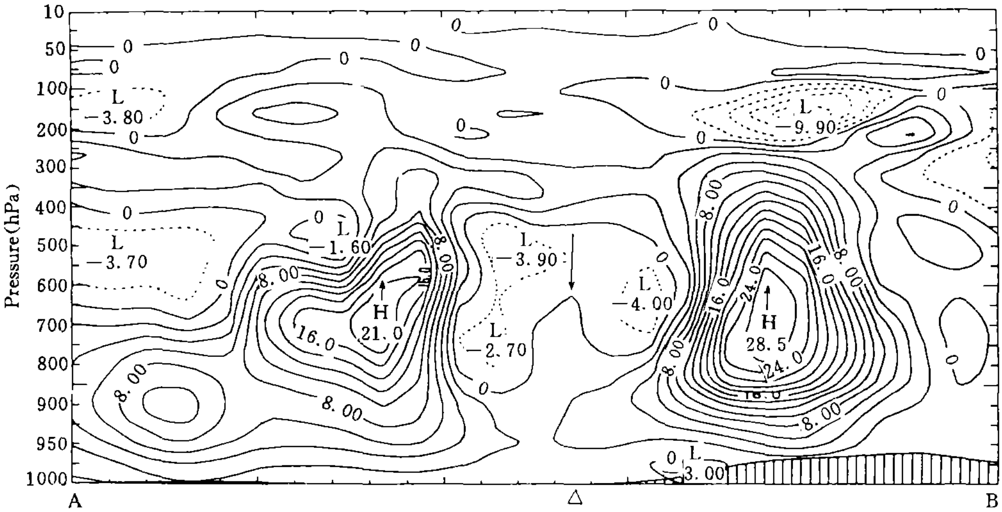

Fig. 6. Vertical cross section of vertical velocity (cm s^{-1}) along AB in Fig. 5d at 0000 UTC 1 August 1996. Δ *indicates the location of typhoon center* (same hereafter).

The cross section of vertical velocity along AB in Fig. 5d shows strong upward motion in the eye-wall from surface up to 300 hPa, with the maximum of 28. 5 cm s^{-1} to the north and 21. 0 cm s^{-1} to the south of eye at 700 hPa: and downward in the center of the eye (Fig. 6). The upward motion in the eye-wall was associated with the divergence field, convergence below and divergence above 800 hPa with the maximum of -2.6×10^{-4} s^{-1} at near 900 hPa to the north of eye.

2. *Thermodynamic Structure near Typhoon Center*

In general, equivalent potential temperature (θ_e) field analyzed from observational data shows relative "warm" in the eye but "cool" in the eye-wall (Liu et al. 1998). Figure 7 shows the 700 hPa geopotential heights at 0000 UTC 1 August and the vertical cross section along CD in Fig. 7a of equivalent potential temperature θ_e anomaly (i. e. difference from the averaged θ_e at same pressure level) analyzed from observational data. Evidently, the typhoon center was relative "warm" (positive θ_e anomaly), with the maximum θ_e anomaly located at 850 and 400 hPa.

The model simulation with higher resolution given in Fig. 8 shows that θ_e in the eye-wall was 7—9 K higher than in the eye at mid-troposphere from 800—500 hPa, hence the typhoon center was relative "cool" (θ_e—344 K) at these levels; at lower levels (950—1000 hPa), however, θ_e in typhoon center was 5 K higher than in the southern eye-wall, hence the center was relative "warm" (θ_e— 351 K). Such a distribution is consistent with the analyses of Hawkins and Imbembo (1976) for hurricane Inez 1966. The "warm" in the eye-wall at mid-troposphere (700 hPa) was associated with the strong upward motion shown in Fig. 6 and higher contents of cloud and rain water, which would release more latent heat (shown later in Fig. 10).

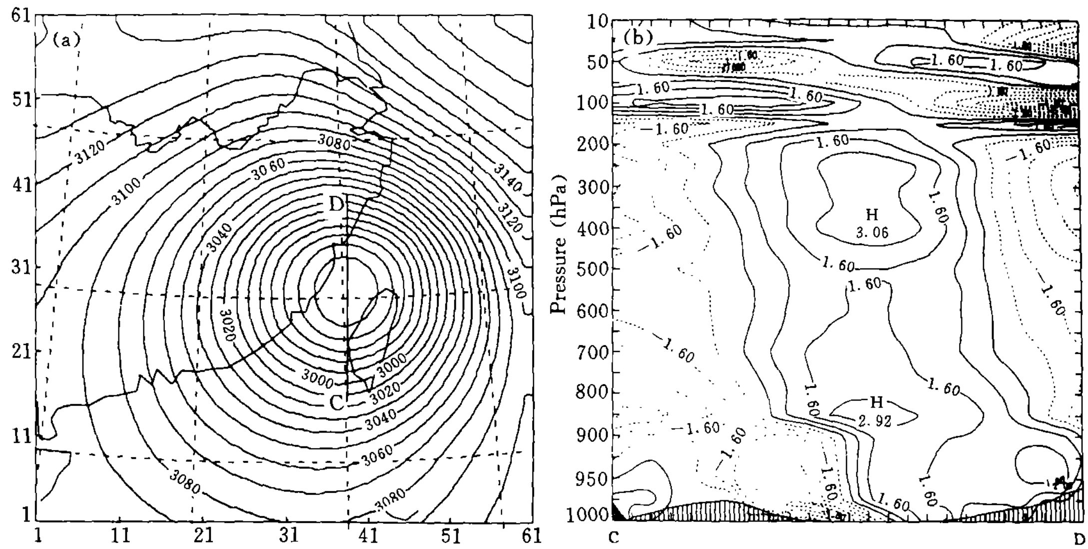

Fig. 7. (a) Objective analyzed 700 hPa geopotential heights (gpm) at 0000 UTC 1 August 1996; (b) Vertical cross section of θ_e anomaly (K) along CD in (a).

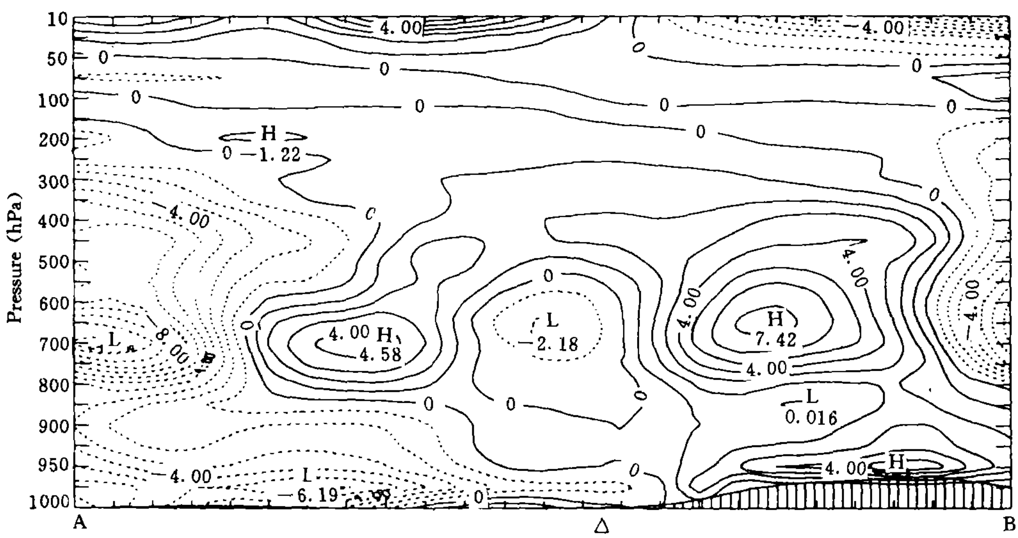

Fig. 8. Vertical cross section of model simulated θ_e anomaly (K) along AB in Fig. 5d at 0000 UTC 1 August 1996.

V. CLOUD AND RAIN PHYSICAL STRUCTURES AND EVOLUTION OF TYPHOON HERB DURING ITS LANDFALL AT TAIWAN AND FUJIAN

In EXPL30 and EXPL10, in addition to water vapor, cloud water and rain water (ice and snow when temperature below 0°C) are also prognostic values. The prognostic equations for water vapor, cloud water (ice) and rain water (snow) mixing ratios are given by the following

$$\frac{\partial P^* q_v}{\partial t} = - m^2\left[\frac{\partial P^* u q_v/m}{\partial x} + \frac{\partial P^* v q_v/m}{\partial y}\right] - \frac{\partial P^* \dot{\sigma} q_v}{\partial \sigma} + \delta_{nh} q_v DIV + P^*(-P_{RE} - P_{CON} - P_{II} - P_{ID}) + D_{qv},$$

$$\frac{\partial P^* q_c}{\partial t} = - m^2\left[\frac{\partial P^* u q_c/m}{\partial x} + \frac{\partial P^* v q_c/m}{\partial y}\right] - \frac{\partial P^* \dot{\sigma} q_c}{\partial \sigma} + \delta_{nh} q_c DIV + P^*(P_{ID} + P_{II} - P_{RC} - P_{RA} - P_{CON}) + D_{qc},$$

$$\frac{\partial P^* q_r}{\partial t} = - m^2\left[\frac{\partial P^* u q_r/m}{\partial x} + \frac{\partial P^* v q_r/m}{\partial y}\right] - \frac{\partial P^* \dot{\sigma} q_r}{\partial \sigma} + \delta_{nh} q_r DIV - \frac{\partial V_f \rho g q_r}{\partial \sigma} + P^*(P_{RE} + P_{RC} + P_{RA}) + D_{qr},$$

where P_{CON} is condensation (freezing for $T<0°C$) of water vapor into cloud (ice) at water saturation, P_{RA} is accretion of cloud by rain (ice by snow), P_{RC} is conversion of cloud to rain (ice to snow) and P_{RE} is evaporation (sublimation) of rain (snow). Additional ice processes are P_{II}, the initiation of ice crystals, and P_{ID} sublimation/deposition of cloud ice. The fall speed of rain or snow is V_f. The term δ_{nh} is 1 for non-hydrostatic and 0 for hydrostatic simulations. D and DIV terms have same meanings as for equation of vertical velocity.

Thus, we can analyze the cloud and rain physical structures and evolution from model simulated fields for cloud water (ice) and rain water (snow). The model simulated cloud and rain water mixing ratio fields show that cloud and rain water were concentrated in the eye-wall but clear in the eye before the typhoon arrived at Taiwan (figures omitted). When the typhoon moved near and passed over Taiwan Island, low-level cloud was developed in the eye. Figures 5b and 5d show the cloud water and rain water mixing ratios at 0000 UTC 1 August at 850 and 700 hPa, respectively. There were no cloud water and rain water in the eye region at 700 hPa, but the eye was filled with cloud water at 850 hPa. Figure 9 shows vertical cross sections through the typhoon center from south to north (Fig. 9a) and from west to east (Fig. 9b) at 1800 UTC 31 July 1996. At this moment the model typhoon arrived in the sea area to northeast of Taiwan Island while the real typhoon had landed over the island (model typhoon was delayed with respect to the real typhoon). From Fig. 9 we can see that cloud had appeared at low-levels but still below 950 hPa in the typhoon center. After the typhoon passed over Taiwan Island, at 0000 UTC 1 August 1996, the cloud had developed up to 800 hPa in the typhoon eye (Fig. 10). The maximum cloud and rain water was located near and above the area of maximum upward motion, where the release of latent heat might form the relative "warm" region in the eye-wall shown in Fig. 8. The low-level cloud developed during the typhoon passing over Taiwan Island made the eye on the satellite cloud picture become fuzzy. Figures 5b and 5d also show that the circle-wise rainband around the typhoon eye consisted of asymmetrically distributed meso-β scale rain cores.

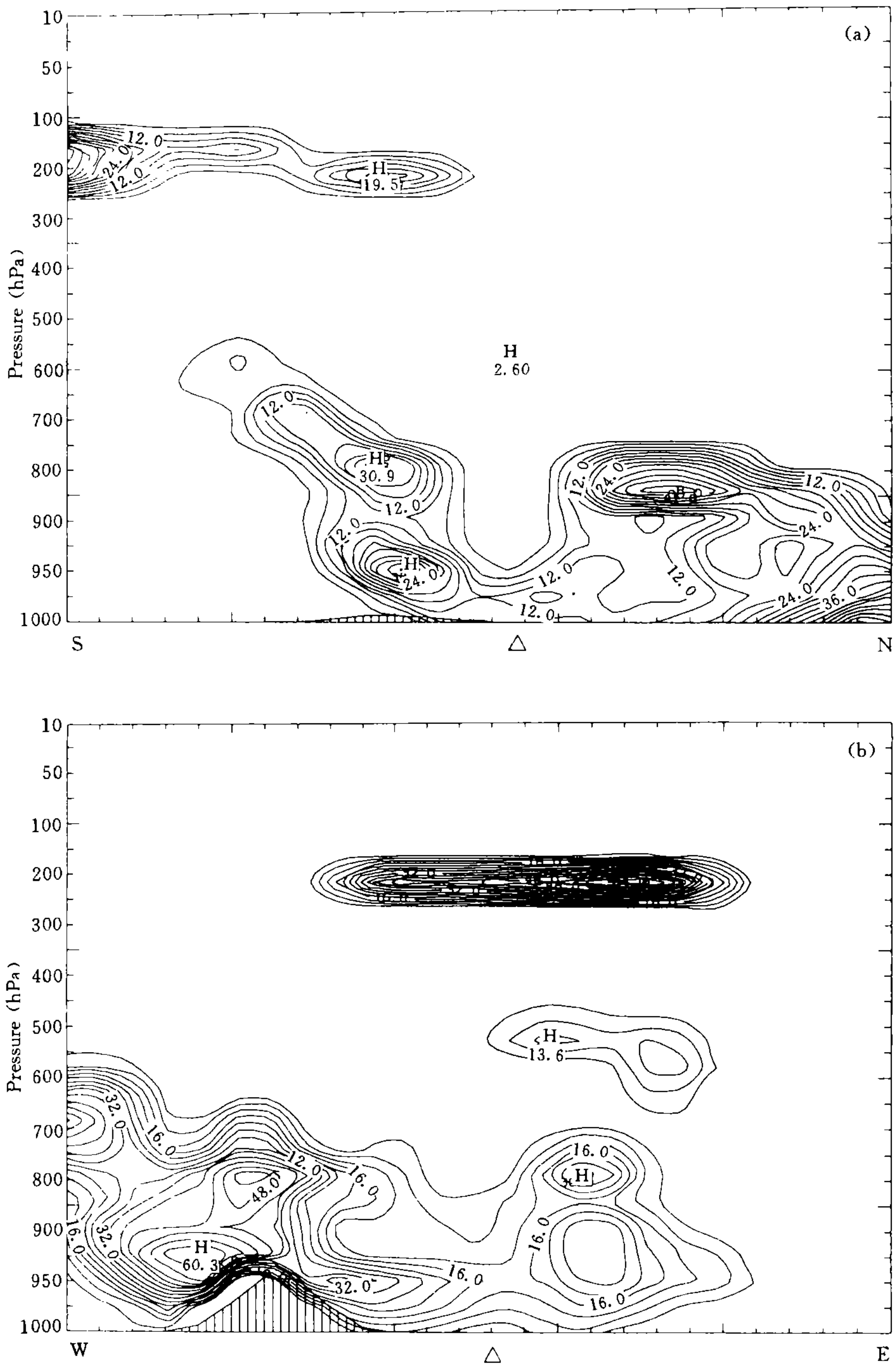

Fig. 9. Vertical cross section of model simulated cloud water mixing ratio (10^{-5} kg kg^{-1}) at 1800 UTC 31 July 1996 (18 h integration) through typhoon center (a) from south to north, (b) from west to east.

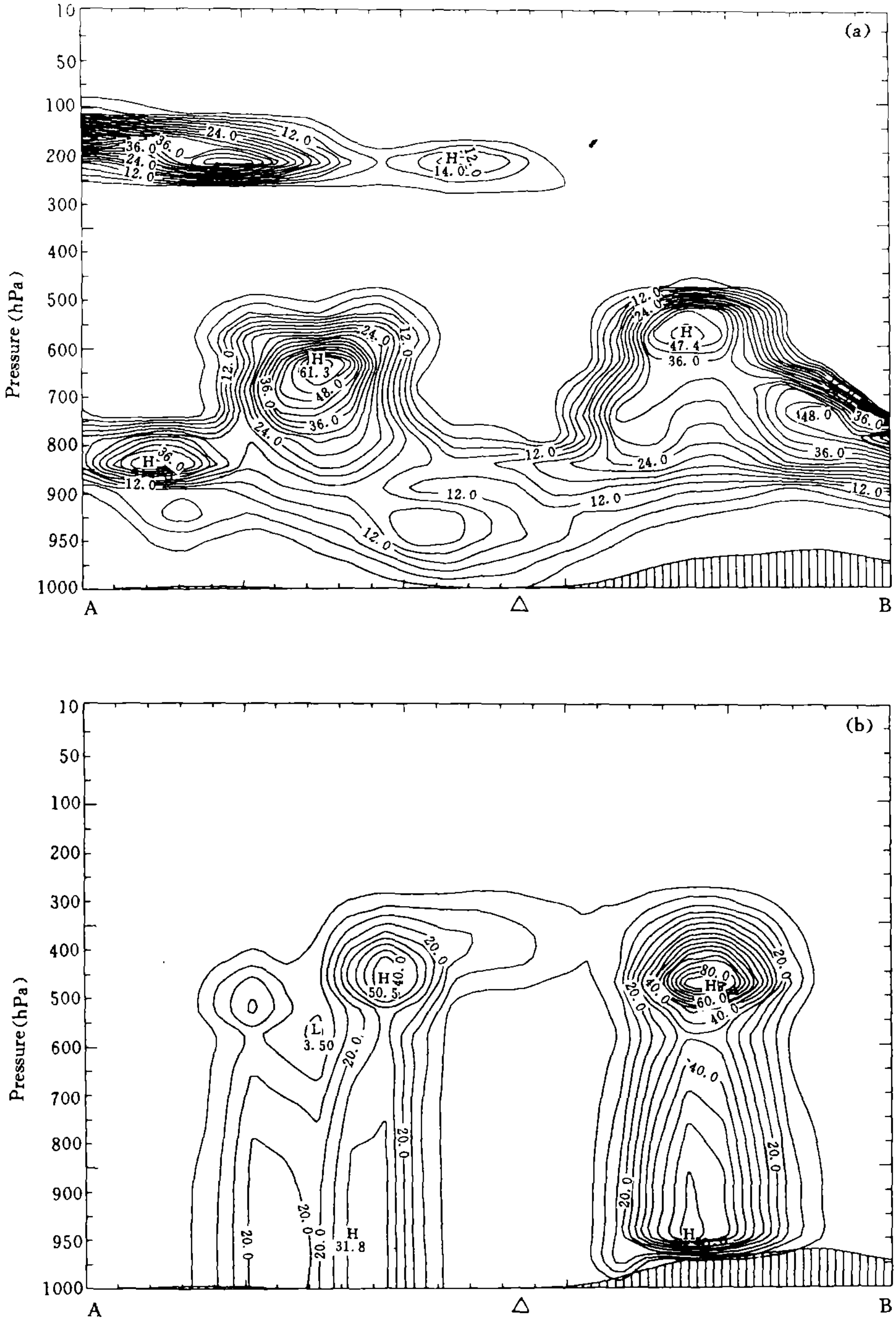

Fig. 10. Vertical cross section of model simulated cloud water and rain water mixing ratios (10^{-5} kg kg^{-1}) through AB in Fig. 5d at 0000 UTC 1 August 1996. (a) cloud water; (b) rain water.

VI. OROGRAPHIC EFFECTS OF TAIWAN ISLAND ON TYPHOON HERB

Experiments EXPL10 and EXPL10-NT were designed mainly for testing the orographic effects of Taiwan Island on the structure of typhoon and heavy rainfall on Taiwan induced by the typhoon. This section will give the major results of this test.

Both EXPL10 and EXPL10-NT revealed major characteristics of dynamic and thermodynamic structures similar to those by EXPL30 discussed above in Section IV. Those include cyclonic inflow at lower levels and outflow at upper levels near typhoon center; asymmetrical wind field structure near the typhoon center and hence the westward motion of the typhoon after landfall; strong upward flow in the eye-wall and downward flow in the eye; etc.

Comparison between simulations "with" and "without" orographic effects of Taiwan Island shows similar conclusion as in Luo and Chen (1995), the effects of Taiwan Island made the typhoon track deviate 30 km away northward after it passed over Taiwan, but there was no obviously impact on the strength of the typhoon.

When the typhoon passed over the island, Taiwan mountain ranged from north to south on the island made the cyclonic circulation be significant confluent along the mountain's sides, especially below 800 hPa. This can be seen from comparison between circulation fields from EXPL10 and EXPL10-NT. Figures 11a, 11b and 11c show streamlines at 850 hPa valid for 1800 UTC 31 July, 0000 UTC 1 August and 0600 UTC 1 August 1996 (integrated 18, 24 and 30 h) for EXPL10, with the orographic effects of Taiwan Island, and Figs. 11d, 11e and 11f for EXPL10-NT, without such orographic effects. The flow began to converge at the central part of the island when the typhoon center was closing to the island from northeast at 1800 UTC 31 July (Fig. 11a). After the typhoon center passed over the island and moved to the seashore near Fujian at 0000 UTC 1 August, the wind was directed towards Taiwan Mountain from west and converged on the ridge of the mountain. At 0600 UTC 1 August, typhoon had moved into the inner-land of Fujian, still with the flow converged over the ridge of Taiwan Mountain, but mainly from the east side. In Figs. 11d, 11e and 11f for EXPL10-NT, there was no such a convergent pattern of flow over the island.

Figure 12 shows model simulated geopotential height, cloud water and rain water at 850 hPa at 0000 UTC and 0600 UTC 1 August by EXPL10 and EXPL10-NT, respectively. Comparing the major features between "with" and "without" orographic effects of Taiwan Island in Figs. 12a and 12c, 12b and 12d, it is found that they are similar and do not have notable orographic effects of Taiwan Island. For example, the isohypses are dense at northeast and loose at southwest quadrant of the typhoon center, which are well agreed with the asymmetric circulation around the typhoon center mentioned before; screw-typed rainband consisted of meso-β-scale rain cores is around the typhoon center; and the typhoon center is filled with cloud and hence the typhoon eye is not clear on satellite picture. However, the orographic effects are clear in the rain pattern over the island: a notable rainband oriented from north to south for EXPL10 in Figs. 12a and 12b (pointed by arrows), versus no such a band for EXPL10-NT in Figs. 12c and 12d.

Figures 13 and 14 show vertical cross sections of divergence, vertical velocity, cloud

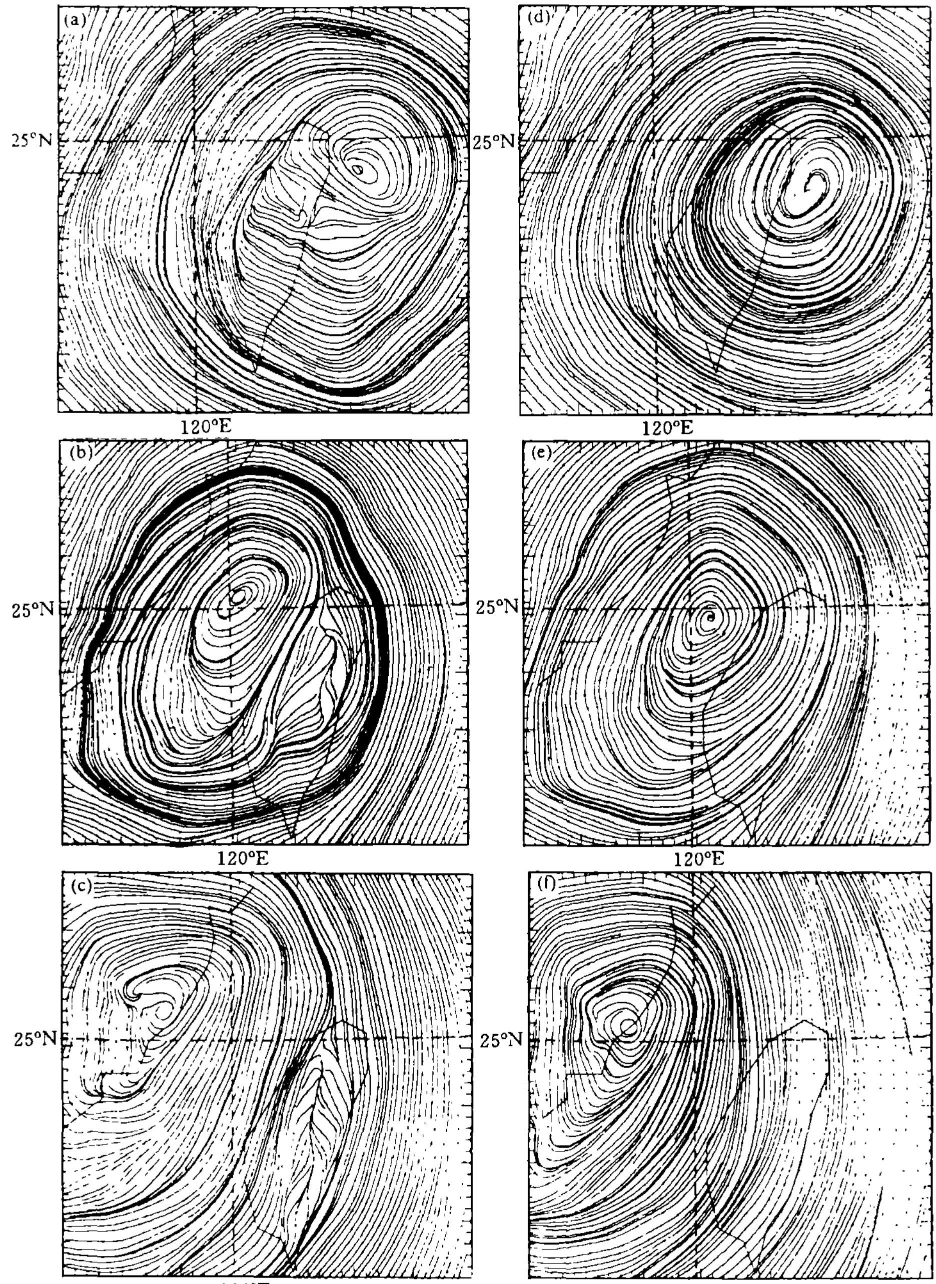

Fig. 11. Model simulated 850 hPa stremline. (a) by EXPL10 at 1800 UTC 31 July; (b) by EXPL10 at 0000 1 August; (c) by EXPL10 at 0600 1 August; (d), (e) and (f) same as (a), (b) and (c), respectively, but by EXPL10-NT.

water mixing ratio and rain water mixing ratio drawn along AB and CD in Figs. 12a and 12b, respectively. Both AB and CD are passing through the maximum rainfall region on the island. We can see from Fig. 13 that flow was converged from both sides (mainly from

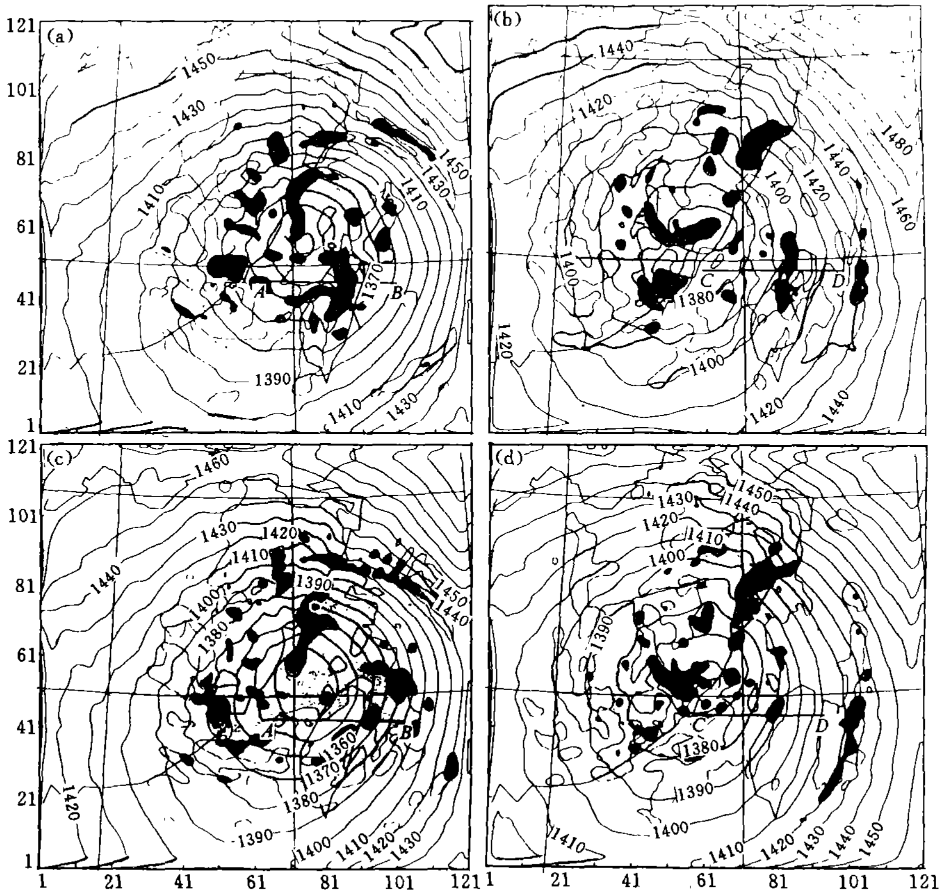

Fig. 12. Model simulated 850 hPa geopotential heights (gpm), cloud water mixing ratio (light shading for $\geqslant 1.0\times10^{-4}$ kg kg^{-1}) and rain water mixing ratio (dark shading for $\geqslant 1.0\times10^{-4}$ kg kg^{-1}). (a) by EXPL10 at 0000 UTC 1 August; (b) by EXPL10 at 0600 UTC 1 August; (c) by EXPL10-NT at 0000 UTC 1 August; (d) by EXPL-NT at 0600 UTC 1 August.

west side at this moment) of the mountain, the maximum convergence over the ridge was -8.7×10^{-4} s^{-1} (Fig. 13a); upward airflow formed by the lifting at the west side and over the ridge, the maximum vertical velocity over the ridge was 85 cm s^{-1} (Fig. 13b): and hence low- and mid-level (up to 600 hPa) cloud developed, and high quantity of rain water appeared over the mountain and touched down to surface (Figs. 13c and 13d). As shown in Fig. 14, the center of typhoon had moved into Fujian Province at this time, the orography of Taiwan Island still impacted flow convergence and lifted the airflow along the sides of the mountain, the maximum of convergence and vertical velocity over the ridge were -5.5×10^{-4} s^{-1} and 72 cm s^{-1}, respectively. In contrast to that shown in Fig. 13, the airflow was mainly converged and lifted from the east side of the mountain instead of from the west side, hence the low-level cloud was also formed over the east side. However high quantity of rain water was still formed over the ridge and touched downward to surface. Later, when the typhoon moved far away from Taiwan Island, the orographic effects of the island were weaken. Till 1200 UTC 1 August, the orographic effects of the island on

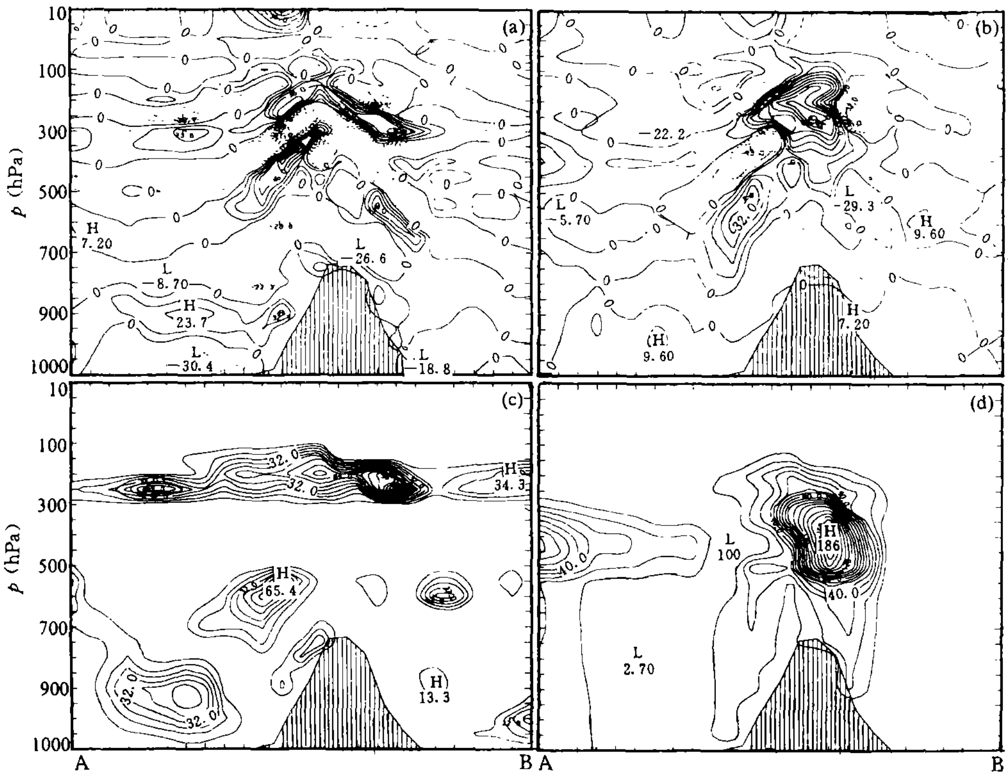

Fig. 13. Vertical cross section along AB in Fig. 12a at 0000 UTC 1 August 1996 simulated by EXPL10. (a) divergence ($10^{-5}\,s^{-1}$); (b) vertical velocity (cm s^{-1}); (c) cloud rain mixing ratio (10^{-5} kg kg^{-1}); (d) rain water mixing ratio (10^{-5} kg kg^{-1}).

the airflow and the rainband over the island could not be seen (figure omitted).

During the period when the typhoon moved near and passed over Taiwan Island within more than ten hours, heavy rainfall was formed on Taiwan Island (Fig. 2c) owing to the lifting of cyclonic airflow by Taiwan Mountain. The vertical cross sections along AB and CD in Figs. 12c and 12d for EXPL10-NT without orographic effects of Taiwan Island show no such confluence and lifting, and hence the cloud and rain maximum over the island (figures omitted). As a result, if no orographic effects of Taiwan Island, the total rainfall in 36 h on Taiwan Island would not have a maximum (Fig. 2d). In comparison, the maximum of 36 h rainfall on Taiwan with the orographic effects of the island (Fig. 2c) was enhanced more than six times with respect to that without orographic effects (Fig. 2d): 269 mm versus 40 mm.

VII. SUMMARY

Numerical experiments of typhoon HERB 1996 were carried out for studying mesoscale structures near the typhoon center during its landfall at Taiwan and Fujian Provinces, and testing the ability of model MM5 to simulate and forecast tropical cyclones. The main results are as follows.

(1) There appear cyclonic inflow circulation on lower levels and outflow on higher

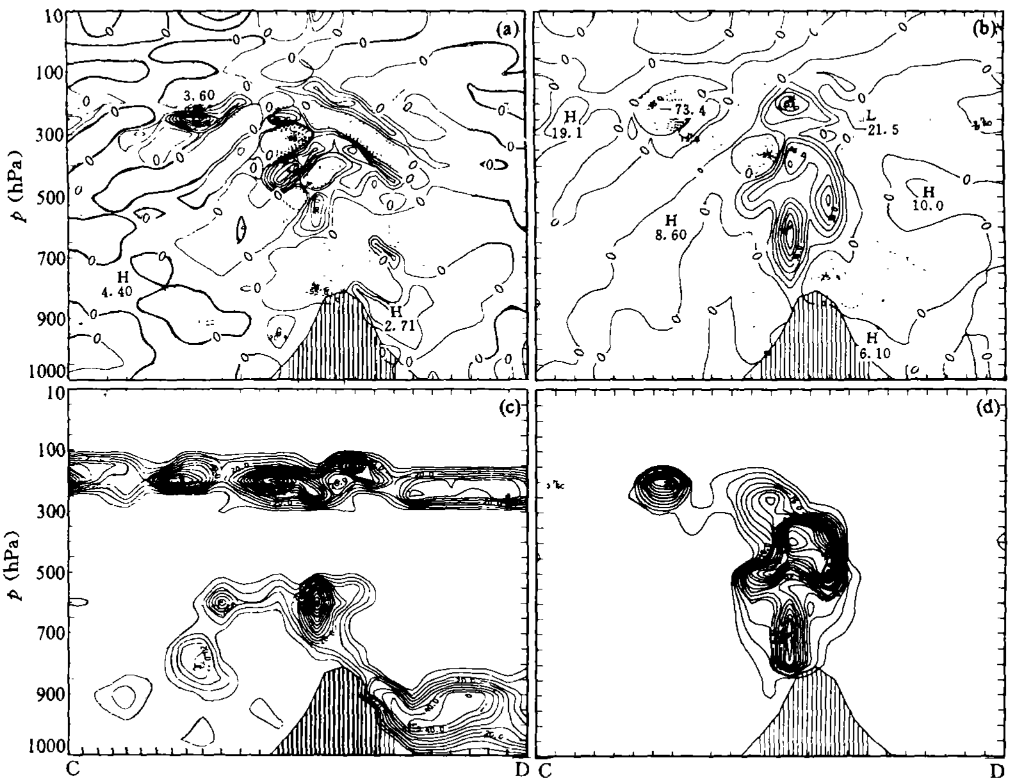

Fig. 14. Same as Fig. 13 except the vertical cross section is along CD in Fig. 12b and valid for 0600 UTC 1 August 1996.

levels near the typhoon center. Strong upward motion formed by low level convergence existed in the eye-wall and subsidence at the center of the eye. Wind field shows clear asymmetrical structure near the typhoon center. The analyses from synoptic-scale observations show that the typhoon center was relatively "warm", but the model simulations with higher space resolution show that at mid-troposphere the eye-wall where existed strong upward motion and more cloud and rain water, was warmer than the eye.

(2) The cloud and rain water were screw-typed or circle-wised distributed in the eye-wall, and consisted of meso-β scale rain cores. During the period of typhoon HERB approaching and passing over Taiwan, the cloud developed at low-levels in the eye region made previous clear typhoon eye on satellite pictures fuzzy.

(3) During the period of typhoon passing over Taiwan and its later landfall at Fujian, the track of typhoon deviated about 30 km northward because of the orographic effects of Taiwan Island, but the strength of the typhoon was not affected obviously. The orographic effects of Taiwan Island caused the cyclonic airflow to converge and lift over Taiwan Mountain, and hence enhanced rainfall on Taiwan Island more than six times.

(4) The non-hydrostatic mesoscale model MM5 has a good ability to simulate and forecast typhoon landfall processes. The model is quite helpful for studying mesoscale dynamic and thermodynamic processes and cloud-rain physical structures associated with typhoon, and it may provide valuable information for landfall forecast of typhoon.

especially on the case when the typhoon eye was not clear on satellite cloud pictures.

REFERENCES

Bender, M. A. et al. (1985). A numerical study of the effects of a mountain range on a landfalling tropical cyclone. *Mon. Wea. Rev.*, **113**: 567—582.

Bender, M. A. et al. (1987). A numerical study of the effects of island terrain on tropical cyclones. *Mon. Wea. Rev.*, **115**: 130—155.

Brand, S. and Blelloch, J. W. (1974). Change in the characteristics on typhoon crossing the island of Taiwan. *Mon. Wea. Rev.*, **102**: 708—713.

Chang, S. W. (1982). The orographic effects induced by an island mountain range on propagation tropical cyclones. *Mon. Wea. Rev.*, **110**: 1255—1270.

Chen Lianshou (1985). The current stage and development of research and operational forecast on motion of tropical cyclone. *Paper Collection of Conf. on Typhoon*. China Meteor. Press, pp. 6 — 30 (in Chinese).

Chen Lianshou and Luo Zhexian (1996). Relationship between asymmetric structure and motion of typhoon. *Paper Collection of Scientific and Operational Experiments and Theoretical Study on Typhoon*. Part 2. China Meteor. Press. pp. 371—374 (in Chinese).

Grell, G. A., Dudhia, J. and Stauffer, D. R. (1994). A description of the fifth-generation Penn State/NCAR mesoscale model (MM5). NCAR Technical Note, NCAR/TN—398+STR, pp. 138.

Hamuro, M. et al. (1969). Precipitation bands of typhoon Vera in 1959 (Part 1). *J. Meteor. Soc. Japan*, **47**: 298—308.

Hawkins, H. F. and Imbembo, S. M. (1976). The structure of a small intense hurricane-Inez 1966. *Mon. Wea. Rev.*, **104**: 418—442.

Liu Huanzhu et al. (1998). Researches on the influence of parameterization of physical process on modeling typhoon and its dynamical structure. *Q. J. Appl. Meteor.*, **9**: 141—150 (in Chinese).

Luo Zhexian and Chen Lianshou (1995). Effects of the orography of Taiwan Island on typhoon tracks. *Sci. Atmos. Sinica*, **19**: 701—706 (in Chinese).

Luo Zhexian et al. (1996). Numerical experiments on the movement of the typhoon Yancy during the SPECTRUM. *Acta Meteor. Sinica*, **54**: 166—174 (in Chinese).

Men Zhiyong et al. (1996). A numerical study of the formation and development of island-induced cyclone and its impact on typhoon structure change and motion. *Acta Meteor. Sinica*, **10**: 430—443.

Xu Xiangde, Chen Lianshou, Xie Yiyang and Kang Di (1996). The asymmetric and dynamic structure of the "β-top" diploe and "ventilation flow" of the target typhoon FLO during TCM-90 field experiments. *Acta Meteor. Sinica*, **54**: 536—543 (in Chinese).

Yeh T. C. and Elsberry, R. L. (1991). Upstream typhoon track deflection caused by the Taiwan orography. *Proceedings of Conf. On Weather Analysis and Forecasting*. April 25 — 27, Taipei, pp. 342—349.

Yang Pingzhang, Wan Qilin and Du Huawu (1996). Numerical study on the orographic effects of Taiwan on the motion of typhoon DOT. *Acta Oceanologica Sinica*, **18**(5): 22—29 (in Chinese).

Zheng Qinglin and Wu Jun (1996). Numerical study of orographic effect on amplication of typhoon precipitation. *J. Nanjing Institute of Meteorology*, **19**: 8—17 (in Chinese).